Supramolecular Chemistry

DOI: 10.1002/ange.201305894

Backbone-Directed Perylene Dye Self-Assembly into Oligomer Stacks**

*Changzhun Shao, Matthias Stolte, and Frank Würthner**

Backbone-supported self-assembly is a versatile, widely used method in supramolecular chemistry.[1–3] In nature, DNA strands self-organize into double-helical secondary structures supported by a backbone composed of sugar and phosphate groups.[4] Similarly, protein backbones organize chlorophyll dyes into efficient light-harvesting complexes in purple bacteria.[5] To mimic the aggregate structures and functions of peptides, proteins, and other natural biomacromolecules, researchers have synthesized and studied artificial foldamers,[6] helical polymers,[7] and DNA-multichromophore systems.[8] However, the production of high-molecular-weight polymers that mimic the sophisticated aggregation process of biomacromolecules still remains a challenge. One difficulty is to understand the thermodynamics and kinetics of complex aggregation processes, which require the determination of the energy levels of self-assembled products, intermediates, and/or transition states.[6,7,9–11]

In our previous work,[12] we introduced perylene bisimide (PBI) dyad **1** (Figure 1), in which the two PBI units are appended to a diphenylacetylene (DPA) backbone to achieve an intramolecular distance of 6.9 Å, exactly twice the space of the PBI π–π interaction. As a consequence of perfect preorganization, this tweezer-like PBI dyad **1** self-assembles into interdigitated dimers with exceptional kinetic stability.[12] We then asked whether, by extending the intramolecular distance in a PBI dyad to triple the space of the PBI π–π interaction, an "arm-in-arm" aggregation into extended PBI π-stacks would be possible.[13,14] According to molecular-modeling studies, spatial control of the triple π–π interactions should be possible by attaching two PBI units at the *meta* positions of a diphenylbutadiyne (DPB) backbone. Thus, we have synthesized the PBI dyad **2**, which possesses these structural features, and studied the self-assembly of this new dyad system.

Herein, we report that the self-assembly of dyad **2** indeed leads to oligomeric PBI stacks through π–π interactions. Furthermore, we found that, unlike the isodesmic aggregation process,[15] the backbone-directed stacking of PBI **2** dyads exhibits cooperative aggregation behavior leading to kinetically stable π-stacks. With thermodynamic and kinetic studies, we were able to derive the whole energy landscape of this self-assembly process.

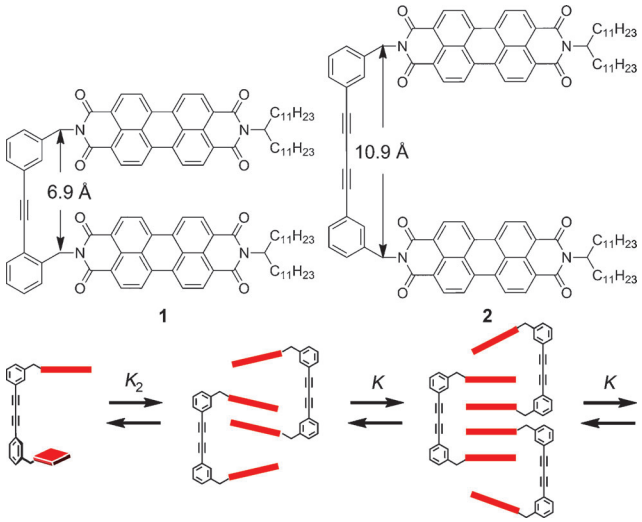

Figure 1. Chemical formulas of PBI dyads **1** and **2**, and a scheme of the backbone-directed arm-in-arm aggregation of PBI **2** into extended oligomeric π-stacks.

The PBI dyad **2** was synthesized in excellent yield by a Cu-catalyzed Glaser homocoupling of the ethinylphenyl precursor PBI **5** (see Supporting Information). Evidence for the self-assembly of PBI dyad **2** into oligomers was obtained using MALDI-TOF mass spectrometry.[16] The sample used for mass spectrometry was prepared by solvent evaporation from a solution of PBI dyad **2** (0.5 mM in methylcyclohexane (MCH)) using 2-[(2*E*)-3-(4-*tert*-butylphenyl)-2-methylprop-2-enylidene]malononitrile (DCTB) as a matrix. Besides the monomer peaks at *m*/*z* 1652, which confirmed the molecular mass of dyad **2**, a series of signals spaced by the same molecular mass (*m*/*z* 1652) was observed in the mass spectrum (Figure 2).[17] Moreover, a careful analysis of the MALDI-TOF spectrum showed as many as 21 peaks, which can be ascribed to the formation of aggregates as large as 21-mers. Because the absorption spectra suggest that the existence of the dyad **2** monomer in the applied sample solution is negligible (see below), the monomers, as well as small aggregates, detected by mass spectrometry should result from the partial fragmentation of large aggregates in the ion source on account of the laser energy and the weak π–π interactions for dyad **2** aggregates.[18] In addition, high-mass ions are usually underestimated from MALDI spectra because of the mass-dependent desorption and detection

[*] Dr. C. Shao, Dr. M. Stolte, Prof. Dr. F. Würthner
Universität Würzburg, Institut für Organische Chemie and Center for Nanosystems Chemistry
Am Hubland, 97074 Würzburg (Germany)
E-mail: wuerthner@chemie.uni-wuerzburg.de

[**] Generous financial support by the DFG for the research training school GRK 1221 "Control of Electronic Properties of Assemblies of π-Conjugated Molecules" is gratefully acknowledged.

Supporting information for this article is available on the WWW under http://dx.doi.org/10.1002/anie.201305894.

© 2013 Wiley-VCH Verlag GmbH & Co. KGaA, Weinheim

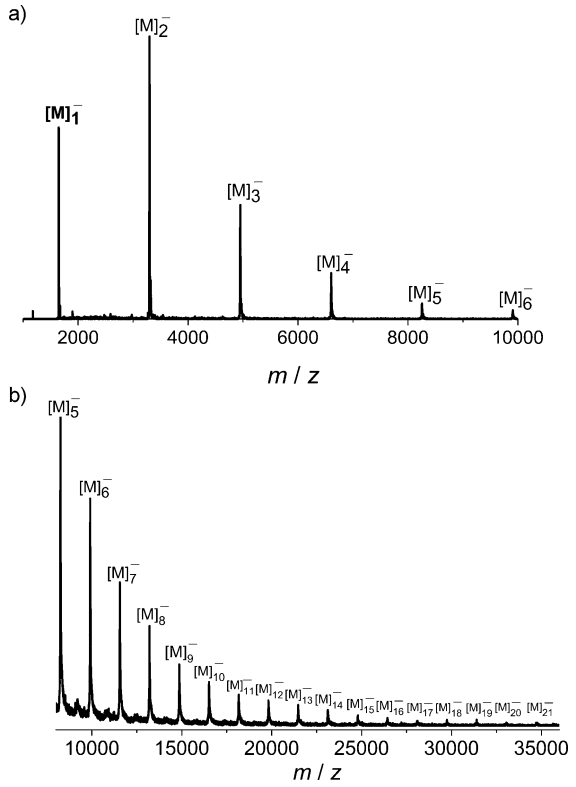

Figure 2. MALDI-TOF mass spectrum (linear mode) of PBI dyad **2**. The peaks corresponding to monomer and aggregate species are marked with $[M]_n^-$ ($n \geq 1$). Both panels are from the same mass measurement; a) shows the *m*/*z* range 1000–10000, while b) shows the *m*/*z* range 10000–35000 with enlarged signal intensities for better visualization.

characteristics of the mass spectrometer.[19,20] These may be the reasons why exponentially decreasing signal intensities for larger species are detected in the mass spectrum, even if large aggregates are the more abundant species in the sample solution.[20]

To assess the aggregate size in solution, a diffusion-ordered spectroscopy (DOSY) NMR experiment[21] was performed with a sample of PBI dyad **2** at a concentration of 0.5 mM in $[D_{14}]$MCH. As depicted in Figure S1 (Supporting Information), the proton NMR spectrum of dyad **2** in this solvent exhibits a complex, broad signal pattern, and the DOSY NMR analysis reveals a translational diffusion coefficient D value of $1.26 \times 10^{-10}\,m^2 s^{-1}$. Both findings are indicative of extended oligomer formation of dyad **2**.[22] Simplistically assuming that the oligomers of **2** are hydrodynamically spherical, the cube root of the molecular weight of the aggregates would be proportional to D^{-1}.[23] Thus, with a PBI reference compound which possesses a similar molecular mass but does not aggregate,[24] the average aggregate size can be estimated according to the equation $N_{DOSY} \approx (D_{ref}/D)^3$. By this method, the average aggregate size of dyad **2** in MCH solution is calculated to be a 20-mer, which is in agreement with the mass spectrometric results.

The aggregation behavior of PBI dyad **2** was first investigated by concentration-dependent ^{1}H NMR experiments in $CDCl_3$ (Figure S2). At all the concentrations applied, a single pattern of proton resonances was observed in compliance with a fast exchange between monomer and aggregate of dyad **2** on the NMR time scale. Upon increasing concentration, the resonances of perylene protons undergo a pronounced up-field shift, indicating π–π interactions of PBI chromophores.[25] On the contrary, the chemical shifts of DPB backbone protons remain almost unaltered between 7.25 ppm and 7.75 ppm (Figure S2). This implies that the DPB units are not involved in π-stacking but reside on the periphery of the PBI π-stacks, revealing the backbone function of the DPB moiety upon aggregation of the PBI dyads.

Because the NMR experiments of PBI π-stacking suffer from either significant broadening (in $CDCl_3$) or a complex pattern of resonance signals (in $[D_{14}]$MCH), we further studied the thermodynamics of the aggregation behavior of dyad **2** by concentration-dependent UV/Vis spectroscopy.[26] By modulating the binding strength in a suitable solvent mixture of "good" chloroform and "bad" MCH,[27] the whole aggregation process of dyad **2** from a molecularly dissolved to a fully stacked species was recorded in the concentration range from 5×10^{-7} to 2×10^{-4} M (Figure 3). Herein, we chose the solvent mixture of $CHCl_3$/MCH ($v/v = 3{:}7$) as the best-suited solvent system for both the thermodynamic and kinetic studies (see below).[26]

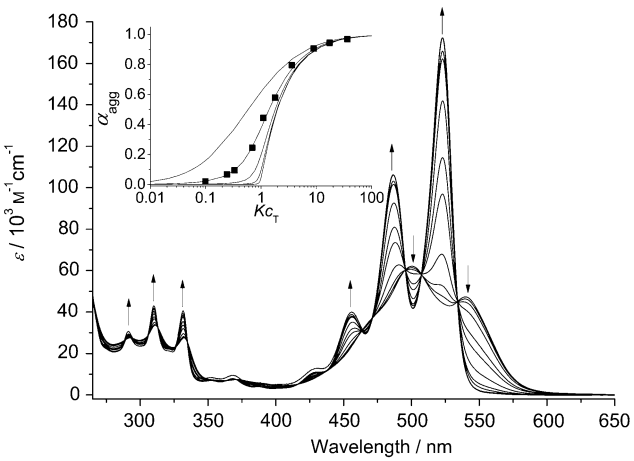

Figure 3. Concentration-dependent absorption spectra of dyad **2** from 5×10^{-7} M to 2×10^{-4} M in $CHCl_3$/MCH ($v/v = 3{:}7$) recorded at 298 K. Each sample was kept at the given concentration for one week to reach the thermodynamic equilibrium (see below). Arrows indicate the spectral changes upon decreasing concentration. Inset: Fraction of aggregated molecules α_{agg} plotted as a function of Kc_T with different $\sigma = K_2/K$ values according to the cooperative model (lines from left to right: $\sigma = 1$, 0.1, 0.01, 0.001, 0.0001), and experimental data points (■).

In general, for the formation of extended PBI stacks from simple PBI monomers the isodesmic model can be applied.[15,22] The concentration-dependent UV/Vis data for the self-assembly of dyad **2** suggest, however, the involvement of some cooperativity.[28] By using the cooperative K_2–K model,[29] equilibrium constants of $K_2 = 18000\,M^{-1}$ for dimerization and $K = 180000\,M^{-1}$ for subsequent growth were

 © 2013 Wiley-VCH Verlag GmbH & Co. KGaA, Weinheim

evaluated (Figure 3, inset). According to the equation $\Delta G° = -RT\ln K$, the Gibbs free energy for the dyad **2** dimerization and subsequent oligomerization can be deduced from the corresponding binding constants to be $\Delta_D G° = -23.9\ \mathrm{kJ\,mol^{-1}}$ and $\Delta G° = -29.5\ \mathrm{kJ\,mol^{-1}}$, respectively. In comparison, the monomeric PBI precursor **5** (Scheme S1) shows only weak aggregation behavior in the solvent mixture of $CHCl_3$/MCH ($v/v = 3{:}7$) with a binding constant of $127\ \mathrm{M^{-1}}$ calculated in terms of the isodesmic model (Figure S3). Thus, at the highest concentration used for PBI **2** (2×10^{-4} M), the degree of aggregation for PBI **5** is less than 5%, while dyad **2** exists nearly exclusively in the aggregated state (less than 4% monomers).

During our studies on PBI dyad **2** self-assembly (see above), we noted increasing equilibration times with increasing MCH content. To quantify the activation energy of dyad **2** self-assembly/disassembly, we carried out kinetic studies by means of time-dependent UV/Vis measurements. Figure 4

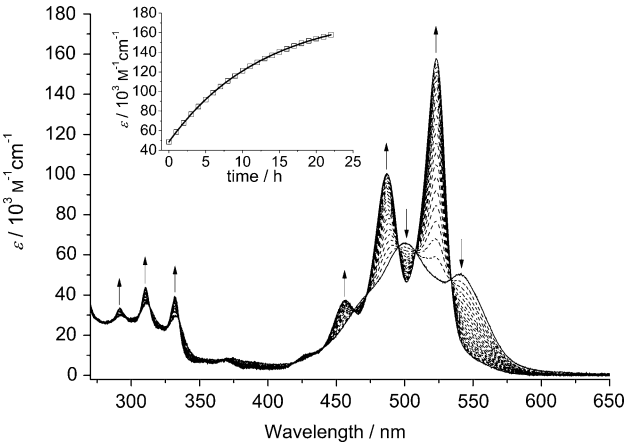

Figure 4. Time-dependent absorption spectra recorded at 1 h intervals for 22 h at 298 K after addition of 7.5 μL of dyad **2** stock solution (2×10^{-4} M) in $CHCl_3$/MCH ($v/v = 3{:}7$) into 3 mL of $CHCl_3$/MCH (v/v=3:7) solvent (final concentration 5×10^{-7} M). The initial aggregate spectrum is highlighted with a solid line. Arrows indicate the absorption changes with time. Inset: Plot of the absorbance at 523 nm versus time.

shows the absorption variations with time upon dilution of a solution of dyad **2** aggregates in the solvent mixture of $CHCl_3$/MCH ($v/v = 3{:}7$) by a factor of 400. In this solvent mixture, the time-dependent absorption changes can be conveniently recorded on a conventional time scale at room temperature.

In these experiments, the stock solution of dyad **2** in $CHCl_3$/MCH ($v/v = 3{:}7$) is 2×10^{-4} M, while after dilution the final solution of dyad **2** in $CHCl_3$/MCH ($v/v = 3{:}7$) is 5×10^{-7} M. At this dilution, the thermodynamically equilibrated state for dyad **2** is as molecularly dissolved molecules, as shown before (Figure 3). The disassembly process can be appreciated from the gradual absorption transition from aggregate to monomer of dyad **2**. Because our thermodynamic studies demonstrated the cooperative self-assembly of dyad **2**, the occurrence of dimers and/or other intermediates should be negligible in this disassembly pathway in accordance with the presence of several well-defined isosbestic points that indicate that only two species are involved, namely the large oligomer and monomer of dyad **2**.

The acquired time-dependent UV/Vis absorption data (Figure 4) can be used to explore the kinetics of the disassembly process of dyad **2**. For details, in particular for the derivation of the equations [Eq. (S1)–(S5)] required for the kinetic analysis, see the Supporting Information. Fitting the measured absorption coefficient $\varepsilon(t')$ values at 523 nm against the measured time t' [see Eq. (S5)] gives exactly an exponential function (Figure 4, inset), confirming that the disassembly process of dyad **2** oligomers into monomers obeys a first-order kinetics. From the fitting curve (Figure 4, inset) the rate constant k of the disassembly process can be deduced to be $0.08\ \mathrm{h^{-1}}$, giving rise to a corresponding half life of $t_{1/2} = 8.66$ h at the given temperature of 298 K.

The same kinetic experiments were repeated at different temperatures. As expected, the rate constant of the disassembly process increases with temperature. The Eyring–Polanyi equation [Eq. (1)] gives a quantitative dependence of the rate constant k on the absolute temperature T:

$$\ln\frac{k}{T} = -\frac{\Delta H^{\ddagger}}{R}\cdot\frac{1}{T} + \ln\frac{k_B}{h} + \frac{\Delta S^{\ddagger}}{R} \qquad (1)$$

where R is the gas constant, k_B is the Boltzmann constant, and h is Planck's constant. From the linear relationship of $\ln(k/T)$ against $1/T$ (Figure S4) the activation parameters $\Delta H^{\ddagger} = 95.4 \pm 2.3\ \mathrm{kJ\,mol^{-1}}$ and $\Delta S^{\ddagger} = -14.0 \pm 7.5\ \mathrm{J\,mol^{-1}\,K^{-1}}$ can be obtained. Thus, for the disassembly process a Gibbs energy of activation $\Delta G^{\ddagger} = 99.6 \pm 2.3\ \mathrm{kJ\,mol^{-1}}$ and an activation energy $E_a = 97.9 \pm 2.3\ \mathrm{kJ\,mol^{-1}}$ of dyad **2** oligomer in $CHCl_3$/MCH ($v/v = 3{:}7$) at room temperature were calculated in terms of Equations (2) and (3), respectively.

$$\Delta G^{\ddagger} = \Delta H^{\ddagger} - T\Delta S^{\ddagger} \qquad (2)$$

$$E_a = \Delta H^{\ddagger} + RT \qquad (3)$$

By combining our results from both thermodynamic and kinetic studies, we can now describe an energy landscape for the self-assembly/disassembly process of dyad **2** in the given solvent mixture (Figure 5). In the thermodynamic studies, the Gibbs dimerization energy $\Delta_D G°$ and the Gibbs free energy $\Delta G°$ for further aggregation of dyad **2** were deduced from the corresponding binding constants K_2 and K to be $-23.9\ \mathrm{kJ\,mol^{-1}}$ and $-29.5\ \mathrm{kJ\,mol^{-1}}$, respectively. The first step of PBI **2** self-assembly can be attributed to the formation of interdigitated dyad **2** dimers, analogous to the self-assembly of dyad **1**.[12] Because of the improper intramolecular spacing in dyad **2** these dimers are not as stable as those of dyad **1** and experience fast exchange with dyad **2** monomers in solution, owing to the low activation barrier $\Delta_D G^{\ddagger}$ (which we could not determine).[30] However, once the dimers of dyad **2** interlocked with each other in an arm-in-arm manner, further assembly into oligomers benefits from the tighter packing with an increased thermodynamic driving force on account of the structural integration (as indicated by a larger binding constant $K > K_2$) leading to the instantaneous

 © 2013 Wiley-VCH Verlag GmbH & Co. KGaA, Weinheim

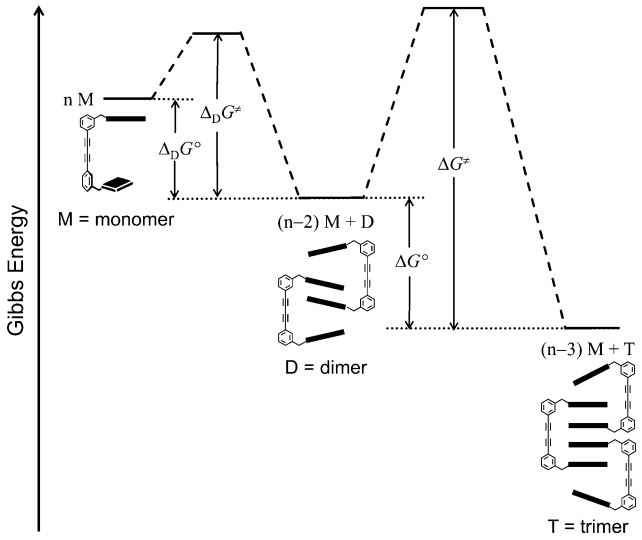

Figure 5. Energy landscape of the self-assembly/disassembly process of dyad **2** in a solvent mixture of $CHCl_3$/MCH ($\nu/\nu = 3:7$) at room temperature. $\Delta_D G°$ and $\Delta G°$ were deduced from the corresponding binding constants K_2 and K to be -23.9 kJ mol^{-1} and -29.5 kJ mol^{-1}, respectively. $\Delta G^{\neq}$ of 99.6 kJ mol^{-1} was determined in terms of the Eyring–Polanyi equation. $\Delta_D G^{\neq}$ was not accessible through our experiments. On the basis of the applied model all further steps of growth into extended π-stacks are characterized by the same Gibbs activation and aggregation energies as shown for the dimer–trimer step.

growth of extended aggregates (on average as large as 20-mers in the given concentration range as evidenced by DOSY NMR).[31]

In the kinetic studies, the dissociation of dyad **2** aggregates was only accomplished by dilution. Thus, the gain in entropy upon dilution afforded the required thermodynamic driving force for a reaction that would be strongly endothermic under standard conditions (i.e. 1M concentration, see Figure 5). To reach the new state of equilibrium, however, dyad **2** aggregates had to overcome an energy barrier $\Delta G^{\neq}$ of approximately 100 kJ mol^{-1} for disassembly at room temperature. Similar to the cooperative aggregate growth revealed by thermodynamic studies and in compliance with the rule of microscopic reversibility, the dissociation of dyad **2** aggregates must also be cooperative, which is supported by the first-order kinetics of the disassembly process and the absence of detectable intermediates such as dyad **2** dimers. Most likely the self-assembly/disassembly process takes place stepwise through the two terminal sides of the dyad **2** aggregates, on account of the less tightly bound outer PBI tweezer unit. According to this model the even less tightly bound dimer nucleus may be formed in a pre-equilibrium process that is characterized by a smaller Gibbs activation energy. In this regard, the kinetic model for the formation of extended PBI stacks closely resembles established models in covalent organic chemistry.

In conclusion, we described the formation of extended PBI oligomer π-stacks by DPB backbone-directed aggregation of PBI dyad **2**. The oligomer stacks of PBI dyad **2** exhibited not only high thermodynamic but also high kinetic stability, and both were observed by using the properly chosen experimental conditions (solvent, concentration, temperature). Accordingly, the energy landscape of the self-assembly/disassembly process of dyad **2** was determined, which provides an in-depth understanding of the backbone-directed PBI self-assembly process. The kinetic stability of the backbone-supported PBI π-stacks should give improved mechanical properties compared to PBI π-stacks composed of simple PBIs[22] and might enable new processing methods for the integration of PBI dyes into organic electronic and photovoltaic devices.

Received: July 7, 2013
Published online: August 13, 2013

Keywords: dyes/pigments · kinetics · self-assembly · π-stacking · thermodynamics

[1] R. Bhosale, J. Misek, N. Sakai, S. Matile, *Chem. Soc. Rev.* **2010**, *39*, 138 – 149.
[2] J. K. Klosterman, Y. Yamauchi, M. Fujita, *Chem. Soc. Rev.* **2009**, *38*, 1714 – 1725.
[3] F. J. M. Hoeben, P. Jonkheijm, E. W. Meijer, A. P. H. J. Schenning, *Chem. Rev.* **2005**, *105*, 1491 – 1546.
[4] J. D. Watson, F. H. C. Crick, *Nature* **1953**, *171*, 737 – 738.
[5] T. Pullerits, V. Sundström, *Acc. Chem. Res.* **1996**, *29*, 381 – 389.
[6] *Foldamers: Structure, Properties, and Applications* (Eds.: S. Hecht, I. Huc), Wiley-VCH, Weinheim, **2007**.
[7] E. Yashima, K. Maeda, H. Iida, Y. Furusho, K. Nagai, *Chem. Rev.* **2009**, *109*, 6102 – 6211.
[8] Y. N. Teo, E. T. Kool, *Chem. Rev.* **2012**, *112*, 4221 – 4245.
[9] D. Thirumalai, G. Reddy, *Nat. Chem.* **2011**, *3*, 910 – 911.
[10] P. A. Korevaar, S. J. George, A. J. Markvoort, M. M. J. Smulders, P. A. J. Hilbers, A. P. H. J. Schenning, T. F. A. De Greef, E. W. Meijer, *Nature* **2012**, *481*, 492 – 496.
[11] T. F. A. de Greef, G. B. W. L. Ligthart, M. Lutz, A. L. Spek, E. W. Meijer, R. P. Sijbesma, *J. Am. Chem. Soc.* **2008**, *130*, 5479 – 5486.
[12] See our previous work: C. Shao, M. Stolte, F. Würthner, *Angew. Chem.* **2013**, *125*, 7630 – 7634; *Angew. Chem. Int. Ed.* **2013**, *52*, 7482 – 7486.
[13] M. Yoshizawa, J. Nakagawa, K. Kumazawa, M. Nagao, M. Kawano, T. Ozeki, M. Fujita, *Angew. Chem.* **2005**, *117*, 1844 – 1847; *Angew. Chem. Int. Ed.* **2005**, *44*, 1810 – 1813.
[14] T. Murase, K. Otsuka, M. Fujita, *J. Am. Chem. Soc.* **2010**, *132*, 7864 – 7865.
[15] Z. Chen, A. Lohr, C. R. Saha-Möller, F. Würthner, *Chem. Soc. Rev.* **2009**, *38*, 564 – 584.
[16] For the application of mass spectrometry in supramolecular chemistry, see: a) B. Baytekin, H. T. Baytekin, C. A. Schalley, *Org. Biomol. Chem.* **2006**, *4*, 2825 – 2841; b) C. A. Schalley, *Int. J. Mass Spectrom.* **2000**, *194*, 11 – 39.
[17] For the application of MALDI-TOF mass spectrometry to determine the π-stacked aggregate formation, see: a) G. Fernández, E. M. Pérez, L. Sánchez, N. Martín, *J. Am. Chem. Soc.* **2008**, *130*, 2410 – 2411; b) K. A. Jolliffe, M. C. Calama, R. Fokkens, N. M. M. Nibbering, P. Timmerman, D. N. Reinhoudt, *Angew. Chem.* **1998**, *110*, 1294 – 1297; *Angew. Chem. Int. Ed.* **1998**, *37*, 1247 – 1251.
[18] a) K. Dreisewerd, S. Berkenkamp, A. Leisner, A. Rohlfing, C. Menzel, *Int. J. Mass Spectrom.* **2003**, *226*, 189 – 209; b) R. Zenobi, R. Knochenmuss, *Mass Spectrom. Rev.* **1998**, *17*, 337 – 366.

© 2013 Wiley-VCH Verlag GmbH & Co. KGaA, Weinheim

[19] a) R. Arakawa, S. Watanabe, T. Fukuo, *Rapid Commun. Mass Spectrom.* **1999**, *13*, 1059 – 1062; b) M. W. F. Nielen, S. Malucha, *Rapid Commun. Mass Spectrom.* **1997**, *11*, 1194 – 1204.
[20] In comparison, the MALDI-TOF mass spectrum of PBI dyad **1** showed only monomer and dimer peaks, see Ref. [12].
[21] Y. Cohen, L. Avram, L. Frish, *Angew. Chem.* **2005**, *117*, 524 – 560; *Angew. Chem. Int. Ed.* **2005**, *44*, 520 – 554.
[22] Z. Chen, V. Stepanenko, V. Dehm, P. Prins, L. D. A. Siebbeles, J. Seibt, P. Marquetand, V. Engel, F. Würthner, *Chem. Eur. J.* **2007**, *13*, 436 – 449.
[23] B. C. Burdett, *Stud. Phys. Theor. Chem.* **1983**, *26*, 241 – 270.
[24] The reference compound used is *N*,*N*′-di(2,6-bis(1-methylethyl)-phenyl)-1,6,7,12-tetra(4-(1,1,3,3-tetramethylbutyl)phenoxy)-perylene-3,4:9,10-tetracarboxylic acid bisimide. See Ref. [22].
[25] a) J. Wu, A. Fechtenkötter, J. Gauss, M. D. Watson, M. Kastler, C. Fechtenkötter, M. Wagner, K. Müllen, *J. Am. Chem. Soc.* **2004**, *126*, 11311 – 11321; b) J. A. A. W. Elemans, A. E. Rowan, R. J. M. Nolte, *J. Am. Chem. Soc.* **2002**, *124*, 1532 – 1540.
[26] C. Shao, M. Grüne, M. Stolte, F. Würthner, *Chem. Eur. J.* **2012**, *18*, 13665 – 13677.
[27] Z. Chen, B. Fimmel, F. Würthner, *Org. Biomol. Chem.* **2012**, *10*, 5845 – 5855.
[28] C. A. Hunter, H. L. Anderson, *Angew. Chem.* **2009**, *121*, 7624 – 7636; *Angew. Chem. Int. Ed.* **2009**, *48*, 7488 – 7499.
[29] T. E. Kaiser, V. Stepanenko, F. Würthner, *J. Am. Chem. Soc.* **2009**, *131*, 6719 – 6732.
[30] The Gibbs activation energy $\Delta_D G^{\ddagger}$ for dimer dissociation should be much smaller than the energy barrier $\Delta G^{\ddagger}$ for disassembly of larger aggregates of dyad **2**. This finding can be attributed to the tight ($\approx$3.5 Å) tweezer-type PBI stacking within dyad **2** aggregates larger than dimers. This tight π–π stacking imposes some steric constraints that need to be overcome in the dissociation process, leading to a substantial Gibbs activation energy.
[31] According to the K_2–K model (for details see Ref. [29]) each integration of a PBI **2** monomer into the oligomeric stack is characterized by the same gain of Gibbs energy, as depicted in Figure 5. Notably, Figure 5 represents the situation under standard conditions (concentrations of 1 M) and not our more dilute experimental conditions where the entropic gain upon dissociation reduces or even inverts the thermodynamic driving force.

© 2013 Wiley-VCH Verlag GmbH & Co. KGaA, Weinheim